Water–air interface deformation by transient acoustic radiation pressure

Félix Sisombat, Thibaut Devaux, Lionel Haumesser, Samuel Callé

Water-air interface deformation by a transient acoustic radiation pressure

Félix Sisombat[1], Thibaut Devaux[1], Lionel Haumesser[1], Samuel Callé[1],

[1]*GREMAN UMR 7347, Université de Tours, CNRS, INSA CVL, 41000 Blois, France*

Corresponding author**:** Félix Sisombat

Contact**:** felix.sisombat@univ-tours.fr

ABSTRACT

The deformation of a fluid interface by the acoustic radiation pressure has been used for surface tension measurements or to design exotic structures such as acoustic diodes. However, few studies focus on the characterisation of the spatial characteristics of the deformation induced by a transient excitation, making research requiring precise spatial control of the deformation challenging. This paper investigates experimentally and numerically the effects of a transient excitation on the deformation generated by an acoustic radiation pressure at the water-air interface. A numerical model using the Finite-Element Method and based on theoretical background for a permanent excitation, is generalized to a transient excitation. An experimental setup is developed to evaluate the maximum height of the interface deformation for different durations and amplitudes of the ultrasonic excitation using two complementary methods: the first using a camera and an edge detection algorithm, the other using a multichromatic confocal displacement sensor. Numerical and experimental results for a non steady-state excitation show a quadratic evolution of the height of the deformation as a function of the incident pressure and also a linear increase as a function of the excitation duration. The evaluation of the deformation height induced by the acoustic radiation pressure at a water-air interface for a transient excitation paves the way to applications requiring noncontact space-time interface modulation, such as subwavelength phenomena.

Index Terms—ultrasound, transient, radiation pressure, interface deformation, experiment, finite-element simulation

I. INTRODUCTION

In past centuries, the concept of radiation pressure has been widely studied in the field of waves physics. In acoustics, Lord Rayleigh developed a new approach to calculate the time-averaged value of the pressure exerted on a piston by a wave with a finite cross section, leading to the first theoretical formulation of the acoustic radiation pressure[1] (ARP). Since this seminal work, several theoretical studies have been dedicated to the formulation of the ARP[2–4], discussing two different approaches of the radiation pressure called Rayleigh radiation pressure and Langevin radiation pressure[5]. First experimental work concerning the interface deformation by the ARP has been carried out by Hertz and Mende[6] for fluid interfaces that are transparent to acoustic waves, showing that the radiation pressure exerted by an acoustic wave on an interface strongly relies

on whether the acoustic beam is bounded or not. Works by Beyer[7] and Chu and Apfel[8] have led to a better understanding of this phenomenon validating Hertz and Mende's results. They paved the way throughout the 20th century for original studies about acoustic streaming[9,10] or acoustic levitation[11–14], and to first experimental works on the dynamic interface deformation[15–17]. Furthermore, these studies lead to various applications such as remote control of implanted medical devices[18], ultrasonic atomization[19] or acoustic tweezers[20]. Recent investigations on the use of the deformation driven by the ARP have been extended to the development of exotic devices such as acoustic diodes and switchs[21]. However deformations using time dependent ARP are most commonly used to characterise the mechanical properties of media without contact[22,23], such as the surface tension of liquids[24–27]. To our knowledge, the relationship of the transient excitation parameters on the size of the resultant interface deformation are not well understood. In particular, the effect of the interfering waves in the cavity formed by the emitter and the interface is rarely considered, making studies requiring knowledge of the spatial properties of the transient ARP induced deformation challenging.

In this way, the main objective of this article is to study the influence of ARP from a non-interfering transient excitation, on the maximum height of the water-air interface deformation. In doing so, a measurement tool is set to predict the maximum height interface deformation for a given set of excitation parameters.

To this aim, based on the theoretical framework of the height of the deformation driven by the ARP for a continuous excitation[17] described in section I, a numerical model using the Finite-Element Method (FEM) is designed. Its description and preliminary results are reported in Section II. Thereafter, the experimental setups designed to measure the maximum height of the deformation using two methods are presented in Section III. The first method is based on image processing of pictures captured with a Digital Single-Lens Reflex (DSLR) camera. The second is based on a confocal multichromatic laser displacement sensor. In the last section, the experimental results obtained by varying the duration of the excitation and the pressure at the interface are shown and compared to simulation results. Finally, the interest of each of the two experimental methods and the validity of the numerical model is discussed.

II. THEORY

1. Radiation pressure

At the interface between two media (Figure 1(a)), the Langevin radiation pressure applied upward at the interface by an unbounded ultrasonic beam normally incident on the interface is equal to the difference in Lagrangian pressure on both sides of the interface[28]: $\Pi(r) = P_1(r) - P_2(r)$

Considering the surface tension σ and the gravity intensity g are opposed to the induced deformation of the interface, the ARP can be expressed as:

$$\Pi(r) = \Delta\rho g h(r) - \sigma\kappa(r) \quad (1)$$

where $\Delta\rho = \rho_1 - \rho_2$ is the density difference between the fluids, $h(r)$ the height of the deformation, $\kappa(r)$ the curvature radius of the interface, is given by:

$$\kappa(r) = \frac{1}{r}\frac{d}{dr}\left(\frac{rh'(r)}{\sqrt{1+h'(r)^2}}\right) \quad (2)$$

Using the expression of the Langevin radiation pressure[7], the acoustic radiation pressure can be expressed as:

$$\Pi(r) = \langle E_1(r)\rangle - \langle E_2(r)\rangle. \quad (3)$$

Figure 1: Deformation of a water-air interface by the acoustic radiation pressure. (a) Schematic representation of the deformation of the interface between two media noted 1 and 2, induced by the radiation pressure at the interface resulting from a normally incident ultrasonic wave. The height of this deformation is noted h(r). (b) Picture of a water-air interface deformation induced by a transient ARP induced by a 1MHz ultrasonic wave focused at the interface (duration 50µs, amplitude 2.5MPa).

Making use of the impedance z_1 and z_2 of the fluids, it is possible to write the energy reflection and transmission coefficients $\mathcal{R} = \left(\frac{Z_1-Z_2}{Z_1+Z_2}\right)^2$ and $\mathcal{T} = \frac{4Z_1Z_2}{(Z_1+Z_2)^2}$, respectively.

These two coefficients allow the mean acoustic energies downstream and upstream at the interface to be written in the following way:

$$\langle E_1(r)\rangle = (1+\mathcal{R})\langle E_i(r)\rangle, \quad (4.1)$$

$$\langle E_2(r)\rangle = \frac{c_2}{c_1}\mathcal{T}\langle E_i(r)\rangle, \quad (4.2)$$

where $\langle E_i(r)\rangle$ is the time-averaged incident acoustic energy density at the interface, c_1 and c_2 the acoustic celerities in media 1 and 2. Thus, from equation (3), the radiation pressure along the interface can be given as follows:

$$\Pi(r) = \frac{2}{c_1}\frac{\rho_1^2c_1^2 + \rho_2^2c_2^2 - 2\rho_1\rho_2c_1^2}{(\rho_1c_1+\rho_2c_2)^2}\langle p_i^2(r,t)\rangle, \quad (5)$$

where ρ_1 and ρ_2 are the densities of media 1 and 2. $p_i(r,t)$ denotes the incident pressure at the interface taking in account both temporal and spatial distributions. In our case, the spatial distribution along the r coordinate is given by the Bessel function of first kind noted J_1.

Under continuous excitation, the pressure incident at the interface is considered to be the pressure at the focal plane of a spherical transducer[29,30] :

$$p_i(r) = 2p_{i0}\frac{J_1\left(\frac{\pi r}{\lambda}\right)}{\frac{\pi r}{\lambda}}, \quad (6)$$

with p_{i0} the incident acoustic pressure at r = 0 and z = 0. This expression is obtained within the parabolic approximation.

Experiments presented in section III have been performed with a 1MHz transducer having an active diameter of 40mm and a focusing at $d_f = 40mm$ (f number f_n=1). To validate the analytical expression (6) describing the spatial pressure distribution at the interface, this theoretical expression has been compared with the pressure radiating by the 1MHz transducer at the focal plane. This pressure field has been measured using a hydrophone (ONDA HGL-0085) in the case of a burst-type excitation (50 cycles of sine wave).

As shown on Figure 2, the Bessel expression of the pressure field correctly describes the main lobe of the acoustic beam at the focal plane of the focused transducer, where the density of energy is at the maximum. Thus, it is convenient to implement this expression of the ARP in the numerical model as an upward pressure at the water-air interface.

Figure 2: Pressure field amplitude at the focal distance along the r axis. Theoretical calculation using equation (6) (solid blue line), and corresponding measurement performed with a hydrophone (orange dotted line) normalized by the maximum pressure at the focal point.

From equation (6), the ARP can be noted:

$$\Pi(r) = 4Cp_{i0}^2\left(\frac{J_1\left(\frac{\pi r}{\lambda}\right)}{\frac{\pi r}{\lambda}}\right)^2, \tag{7}$$

with $C = \frac{1}{\rho_1 c_1^2}\frac{\rho_1^2 c_1^2 + \rho_2^2 c_2^2 - 2\rho_1\rho_2 c_1^2}{(\rho_1 c_1 + \rho_2 c_2)^2}$. It is therefore possible to obtain the analytical formulation of the surface displacement $h(r)$ induced by the ARP, which is the subject of the following subsection.

2. Analytical formulation of the interface displacement

From the formulation of the acoustic radiation pressure given by equation (7), using a Hankel transform[31], it is possible to express equation (1) as follows:

$$(\Delta\rho g)\tilde{h}(k) - \sigma\tilde{\kappa}(k) = 4Cp_{i0}^2\tilde{\phi}(k), \tag{8}$$

with $\tilde{\phi}(k)$ the Hankel transform of the spatial distribution $\phi(r) = \left(\frac{J_1\left(\frac{\pi r}{\lambda}\right)}{\frac{\pi r}{\lambda}}\right)^2$.

In this work, we assume small deformations of the water-air interface, allowing to reduce equation (2):

$$\kappa(r) = \frac{1}{r}\frac{d}{dr}\left(rh'(r)\right) = \Delta_r h(r). \tag{9}$$

The Hankel transform of the cylindrical Laplacian is noted $\widetilde{\Delta_r} f(k) = -k^2\tilde{f}(k)$. The height of the deformation can therefore be expressed as follows[17]:

$$h(r) = \frac{2\lambda^2}{\pi^2}Cp_{i0}^2\int_0^{\frac{2\pi}{\lambda}}\frac{1}{\Delta\rho g + \sigma k^2}\left(1 - \frac{\lambda k}{\pi^2}\sqrt{1 - \frac{k^2\lambda^2}{4\pi^2}} - \frac{2}{\pi}\arcsin\left(\frac{\lambda k}{2\pi}\right)\right)J_0(kr)kdk, \tag{10}$$

with $\tilde{\phi} = \frac{\lambda^2}{2\pi^2}\left(1 - \frac{\lambda k}{\pi^2}\sqrt{1 - \frac{k^2\lambda^2}{4\pi^2}} - \frac{2}{\pi}\arcsin\left(\frac{\lambda k}{2\pi}\right)\right)$ for $k \leq \frac{2\pi}{\lambda}$, 0 either. From equation (10), it can be observed that a number of parameters can affect *h(r)*: the surface tension σ, the wavelength λ and the amplitude p_{i0} at the focal point. Moreover, it can be expected that the height of deformation varies with the square of the input pressure p_{i0}. This will be discussed in the following part where the solution of this equation is compared to numerical results.

III. METHOD

To investigate the influence of the excitation parameters on the height of the interface deformation induced by the ARP, a numerical model using FEM has been adapted and a dedicated experimental setup has been developed.

III.1 Numerical Model

a. Continuous excitation

The influence of the amplitude p_{i0} at the focal point on the height of the deformation is studied using a finite element software[32,33] (COMSOL Multiphysics®). The model allows to focus on the time evolution of the deformation and the influence of the physical fluid parameters. The module "laminar two phase-flow, moving mesh" is used to solve the Navier-Stokes equation for an incompressible flow. This method is used to compute the displacement of the interface between two fluids. The model shown on Figure 3 is built using a 2D-axisymmetric geometry and is bounded by three types of boundaries.

i) A free surface with an external force is applied in +z direction, corresponding to the acoustic radiation pressure described by equation (6). To reduce the weight of calculations, the upper fluid (air) is not represented in the model. As an alternative, its effect is depicted by the surface tension of a water-air interface and added to the free surface boundary condition (represented by the yellow line on Figure 3).

ii) The ARP is calculated along the r-axis using the pressure distribution given by equation (6), making use of the characteristics of the transducer used for the experiments described in section III.2 (1MHz for frequency, 40mm in diameter, focal distance of 40mm).

iii) The no slip wall boundary condition is used to specify stationary solid walls of the water tank (solid blue lines in Figure 3). Moreover, the right end side of the computation domain is set large enough (6 mm) to avoid interactions between the deformation and the reflected waves by the water tank walls before that the interface deformation reaches its maximum amplitude. Moreover, the thickness of the model has to be larger than the negative amplitude of the surface displacement. It is set larger than twice the maximum water level elevation at $r = 0$.

Despite the absence of an air layer above the water in the numerical model, the model takes into account the atmospheric pressure as well as the gravity effects. As the interface is deformed, the moving mesh used to study the motion of the water surface governs the shape of the water domain. The minimum size of an element of the moving mesh is 1µm, so the mesh displacement is fine enough to describe the excitation pressure field at the interface along the *r*-axis and the interface deformation which can vary from about 50µm to 1mm depending on the applied ARP along the *z*-axis. The time resolution is set to 10µs to obtain an adequate sampling of the mesh displacement in time (1000 points over the rise time). The surface displacement along the *z*-axis is calculated and the maximum value of this displacement is picked up at $r = 0$ for different pressure levels p_{i0}.

Figure 3: Fluid dynamics FEM model. A 2D axisymmetric geometry is used (the revolution axis is the red dashed line) with no-slip boundary condition (blue lines) on both walls. On the water-air interface (yellow line), an external force is applied along the z+ direction. Case of (a) an external force considered as null and (b) given by equation (7) corresponding to the acoustic radiation pressure for a continuous excitation with $f = 1MHz,\ p_{i0} = 250kPa$.

The simulations are first performed for an ARP corresponding to a steady state excitation, denoted by equation (7), and are compared to theoretical results obtained using equation (10). The maximum deformation height as a function of the square of the incident pressure is reported on Figure 4. A good agreement is found between simulation (red dots) and analytical (blue dots) results for acoustic pressures below 2.5×10^4 kPa^2 (orange dashed lines on Figure 4). The quadratic dependence is shown by the black dashed line on Figure 4, and confirms the Langevin radiation pressure theory for the small deformation case[11,12]. For higher pressures, there is a divergence between the results since the theoretical model quadratic assumption is no longer valid. The maximum height of the deformation tend to increases as a cubic law of the pressure as discussed by Nomura and Shimomura[34]. It shows that the analytical formulation using the hypothesis of small deformation (equation 9) is no longer valid in this range of pressure. The FEM model being validated with theory in the case of a continuous excitation, it is now extended to the case of a transient excitation.

b. Transient excitation

To predict the height of the deformation of an interface by a transient excitation, the time dependence of the input pressure at the interface should be included into the expression of the incident pressure p_i (equation (6)). Thus, the time-dependent ARP can be noted:

$$\Pi(r,t) = 4Cp_{i0}^2 \left(\frac{J_1\left(\frac{\pi r}{\lambda}\right)}{\frac{\pi r}{\lambda}} \right)^2 H(\tau - t)H(t - t_0), \tag{11}$$

where $H(t)$ is the Heaviside function and $\tau - t_0$ the excitation duration.

Figure 4: Numerical results for a continuous excitation (a) Comparison of the maximum deformation height induced by the acoustic radiation pressure given by equation (7) (blue dots) as a function of the square of the pressure level, and FEM simulations (red dots). (b) 3D view of a simulation result for $p_{i0} = 140kPa$ (orange dashed lines). A maximum deformation height of 0.11 mm is reached.

In this study, we exclusively consider a water-air interface. Only three parameters can influence the value of the radiation pressure: the pressure at the focal point p_{i0}, the duration of the excitation $\Delta t = \tau - t_0$ and the wavelength λ. As the frequency is set to f = 1MHz, this study focuses on the influence of the input pressure and the duration of the transient excitation. As the theoretical formulation of the height of the deformation induced by a transient ARP proposed by Ostrovakia[35] relies on small deformation hypothesis, experimental results in the following sections will only be compared to the numerical model that does not make this assumption. In that

way, the developed numerical model enables a broader use than known analytical model[35] that is needed in section IV. Further, it gives access to various physical settings, such as the number of sources, which could be useful to compare further analytical works about transient ARP at an interface, without the small deformation assumption.

III.2 Experimental setup

Experiments are carried out in a tank filled with water as shown in Figure 5. During the experiment, the water temperature is 20°C. A burst electrical signal made of sine periods of 1µs, delivered by a RITEC RAM 5000 ultrasonic pulser, is applied to a 1MHz NDT SYSTEM IDH018 piezoelectric transducer, with a duty cycle varying from 0.0015% to 0.105% depending on the burst duration. The transducer (40 mm active diameter) emits an acoustic beam focused on a water-air interface (focal distance $d_f = 40$ mm). Two devices are used to simultaneously measure the height of the deformation induced by ARP*:*

i) a confocal laser displacement sensor pointing the deformation,

ii) a camera with a macro lens for capturing the deformation of the interface.

The camera is a Digital Single-Lens Reflex (DSLR) camera NIKON D5600. It uses a CMOS sensor of dimensions 23.5x5.6mm^2 which enables a resolution of 6000x4000pixels. The camera is used with a Tamron SP90mm macro lens, and images are taken setting a shutter speed of 1/4s (0.25s) and an aperture F/22 (4mm). The ultrasonic excitation is emitted 20 times per second, the resulting photograph is an average over 5 deformations over the time of exposition of the camera's sensor. This provides higher brightness at the edges of the deformation and favors to capture the top of the deformation. The camera is placed 30 cm away from the deformation, outside of the tank. Due to the presence of a meniscus of water on the edges of the water tank, a tilt angle $\alpha \approx 5°$ is set to capture the deformation. A ruler is placed beside the deformation to measure the length of one pixel. The resulting photograph is processed in order to get the maximum height of the deformation. This process includes three steps, as presented on Figure 6. First, the size of one pixel is evaluated. Then the image is cropped around the deformation to reduce the calculation domain. Finally, a Canny edge detection[36] is performed to extract the edge of the deformation. This is a multi-step algorithm for locating net intensity gradient changes in an image filtered by a Gaussian operator for denoising.

Figure 5: Experimental setup to measure the height of the deformation. A broadband ultrasonic transducer placed at a distance *d* from the interface is used to generate a transient ARP. The deformation of the water/air interface is captured with a camera Nikon D5600. Photos are post-processed with an edge detection algorithm to evaluate the maximum height of the deformation. In parallel, the deformation is also measured by a multichromatic confocal laser displacement sensor (KEYENCE CL-3000) which tracks the top of the deformation at any time.

From the edge detection and the size of one pixel, it is possible to compute the height of the deformation induced by the ARP. This method allows one to have an overall view of the interface deformation and ensures a right detection of the top of the deformation. As the camera is tilted at $\alpha \approx 5°$, an underestimation of the height of the deformation is expected and increases as the height of the deformation decreases (up to 30µm), as shown

in Figure 6(b). Due to this angle, the bottom of the deformation cannot be accurately estimated as highlighted in Figure 6(c).

In parallel, a method using a multi-wavelength confocal displacement sensor[37] (KEYENCE CL-P070) and its controller (CL3000) is used to evaluate the height of the deformation on a single spot of 50µm in diameter. The diameter of the spot is small enough compared to the curvature radius at the top of the deformation so the resulting measurements are the average of the maximum height of the deformation over the surface of the spot (Figure 5). The sensor head is placed 70mm above the water surface in the vertical to the measurement spot. It allows a measurement range of ±10mm of the surface displacement with a sampling frequency of 10kHz. Methods using a laser probe to measure the displacement of optically transparent interfaces have already been used in the literature to measure the properties of fluid-like surfaces[16,24,25]. It allows a high resolution ($\pm 2\mu m$) to measure small deformations as the camera becomes inaccurate. In the following section, experimental and numerical results are investigated for different input pressures levels and excitation durations.

Figure 6: Evaluation of the deformation height using the camera. (a) First, a ruler graduated in mm is set to evaluate the size of one pixel. An edge detection algorithm is used to calculate the gap between the top h_{max} and the bottom h_0 of the deformation. (b) Error in the estimation is expected because of the view angle α of the camera. (c) The position where the base of the deformation is set (h_0) is located on the interval delimited by the solid blue lines (width of approximately 50µm), due to reflection of light on water and angle of inclination, impacting on the accuracy of the measurement.

IV. RESULTS AND DISCUSSION

IV.1 Evolution of the deformation amplitude as a function of the input pressure

To study the influence of the incident pressure, experiments have been carried out placing the transducer at a distance from the interface equal to its focal length ($d = d_f = 40$mm) with an excitation duration equal to 30µs, while increasing the incident pressure p_{i0} from 1.5 MPa to 5.7 MPa. These parameters are chosen to evaluate the height of the deformation by at least one of the measuring methods. For the camera, the minimum height of deformation that can be measured is limited by the spatial resolution of the camera (5µm per pixel, at least 3 pixels are required to distinguish the edges of the deformation) and the tilt angle.

Due to the waves in the tank caused by parasitic vibrations in the room, the minimum deformation height that can be measured with the laser probe is not less than 40µm. Beyond that value, measurements become too noisy. Figure 7(a), shows that the experimental height at $r = 0$ are in good agreement with the simulation ones. It is possible to see that the camera-based method (blue triangle symbols), struggles to measure deformations of less than 0.2 mm height. As expected, the laser probe (red square symbols) is able to detect deformations height down to 40µm. When increasing the pressure above 4 MPa, for 30µs excitation duration (duty cycle of 0.045%), water atomization occurs: small droplets are projected above the interface deformation which lead to an incorrect estimation of the interface deformation preventing measurement of the top of the deformation with the laser probe. In this particular situation, the camera-based method is still reliable, although it is necessary to adapt manually the threshold of the edge detection algorithm from the picture of the deformation, so the droplets can

be ignored. Results from both methods highlight an increase of the deformation height as a function of the square of the incident pressure, which is represented by a red dashed line on Fig.7. This dependence corresponds to the theory given by equation (10) and also by the first experimental observations carried out by P.L. Marston for an acoustic levitated drop in water driven by modulated radiation pressure[14,38–40]. However, due to the use of a perfectly rectangular windowing of the excitation durations during the simulations, the computed mean pressure over time at the interface is slightly superior than the experimental one. As a result, the experimental heights are lower than those obtained with the numerical model.

Figure 7: Deformation height as a function of the input pressure. Comparison of measurement and simulation results for (a) an incident pressure p_{i0} from 1.5 MPa to 5.7 MPa with an excitation duration Δt of 30µs and (b) incident pressure p_{i0} from 1.2 MPa to 3.5 MPa with an excitation duration Δt of 50µs. Solid black line shows the results from simulations. Red dashed line exhibits the quadratic fit from the measurement performed with the laser probe (square symbols). Triangles symbols show results obtained with the camera and edge detection algorithm.

To ensure that the quadratic behaviour is still relevant when increasing the excitation duration, a second measurement is performed with an excitation duration of 50µs (duty cycle of 0.075%), while increasing the incident pressure p_{i0} from 1.2 MPa to 3.6 MPa (Figure 7(b)). Results show once again a good agreement between simulations and experiments, proving that if the transient excitation duration is less than 50µs, the maximum height of the deformation increases as a square law of the pressure. It can be observed that for an input pressure of 3MPa, the maximum height of the deformation is approximately equal to 0.25mm and 0.40mm for an excitation duration of 30µs and 50µs respectively. It seems to shows a linear evolution of the deformation height as a function of the transient excitation duration, which is the subject of the following section.

IV.2 Evolution of the deformation amplitude as a function of the excitation duration

Experiments and simulations have been carried out for an excitation duration in the range of Δt = [1, 54]µs (duty cycle varying from 0.0015% to 0.081%), which ensures to have transient non overlapped excitation, with a pressure $p_{i0} = 3.5MPa$. The latter allows to obtain a deformation height greater than 0.5µm for shortest excitation duration, so it can be detected by the laser probe. The results are reported on Figure 8(a). As expected, simulation results (solid black line) highlight a linear dependence when the excitation duration Δt increases. Red squares illustrate that measurements from the laser probe are in good accordance with the simulation while the excitation duration remains inferior to 54µs. The linear fit (red dashed line) highlights a slope of 10.4µm/µs which is close to the simulation one (10.84µm/µs).

Figure 8: Deformation height as a function of excitation duration. (a) Comparison of measured and simulated heights of deformation for $p_{i0} = 3.5$MPa at f = 1MHz. The black solid line shows the results from simulations, squares and triangles show experimental results obtained with the optical probe and the camera, respectively (b) Picture of the water-air interface deformation for Δt = 54µs and p_{i0} = 3.5 MPa at f = 1MHz.

Results from the camera (blue triangles) also match to the simulation results while the maximum height of the deformation is greater than 0.25mm ($\Delta t > 30$µs) (Figures 8(a-b)), with an underestimation compared to

the numerical result due to the time windowing of the input excitation. For emission durations between 18 and 30µs, the interface deformation is still detected, but a miss estimation of the height is due to the tilt angle of the camera, resulting in a under estimation of the deformation as its heights decreases, until a threshold of $\Delta t < 18$µs, where the interface deformation cannot be evaluated anymore, even if it remains observable.

IV.3 Influence of the distance between the transducer and the water-air interface

To study the influence of the distance between the transducer and the water-air interface relatively to the burst duration, the transducer is set at a distance d = 30mm from the interface and is moved away from the interface along the z-axis up to d = 50mm. The maximum height of the interface deformation is measured with the optical probe as it allows to measure smaller deformations. The signal emitted by the transducer is described in section III.2, with an amplitude of 2.1MPa: it ensure no atomization of water when investigating the excitation duration range Δt = [20, 70]µs (duty cycle varies from 0.03% to 0.105%).

The height of the deformation induced by the ARP measured while moving the transducer along the distance d = [30mm, 50mm], for four excitation durations and is shown on Figure 9 (a). It can be observed that the maximum height is globally located at the focal distance ($d = d_f = 40mm$) regardless of the duration of the burst. However, at this distance, when $\Delta t > 56$µs, the height of the deformation doesn't increase linearly as expected from section IV.2.

Figure 9: Transition from a transient state to an interference regime (a) Influence of the cavity length (distance between the transducer and the water-air interface) on the height of the deformation for different excitation duration with p_{i0} = 2.1 MPa. (b) Picture of the water-air interface for Δt = 150µs and p_{i0} = 2.1 MPa. A "tether like" shaped deformation can be observed.

This is due to the excitation duration being greater than the time of back and forth travel path for returning to the transducer, establishing a steady state in the cavity of length d formed by the transducer and the interface ($\Delta t \geq 2d/c$) . This effect of interferences is confirmed in figure 9(a): when increasing the excitation duration.

The observed interferences show maxima every λ/2 = 0.75mm, corresponding to the results obtained by Kornfeld and Triers[41]. These strong variations over short distances can be difficult to control experimentally over times where water can evaporate and hence change the interference pattern (blue and green dotted lines). For example, it can be noticed that for Δt = 70µs at around d = 35mm, the maximum height of the deformation can change from simple to double. When increasing the excitation duration up to 150µs, the shape of the deformation shifts from Gaussian to a tetter-like shape as shown on Figure 9(b). This situation is beyond the scope of this work in which the transient regime yields smooth variations of the deformation height over time (black and red dotted lines).

V. CONCLUSION

In this study, we have investigated the water-air interface deformation generated by the acoustic radiation pressure for a transient non-overlapped excitation.

A numerical model has been developed to predict the maximum height of deformation as a function of the excitation duration and the input pressure of the incident wave. The numerical model validity was confirmed by comparison to an analytical formulation in the case of a harmonic excitation. The quadratic dependence of the deformation height was confirmed at small excitation levels. Moreover, in the case of a harmonic excitation, a cubic dependence was shown for higher pressure levels ($p_{i0} > 140\text{kPa}$) which confirms the work of Nomura[34].

Two complementary experimental methods have been proposed to measure the height of deformation. Firstly, the method using a camera fails to measure small size deformations but gives a good overview of the shape of the deformation. Further, it allows to check the formation of droplets. when the measurements provided by the confocal displacement sensor are inconsistent. Secondly, the method using the confocal displacement sensor provides a more accurate measurement of the height of the deformation, measuring in the lower range starting from 40μm. However, the measurements are inconsistent in the presence of droplets.

Results show that the height of deformation increases with the square of the incident pressure, and increases linearly with the excitation duration for a non-interfering transient acoustic excitation of duration $\Delta t \leq 2d_f/c$. Results are in good accordance with the numerical model, stating that it is convenient to predict in that way the height of the deformation induced by a transient acoustic radiation pressure. Furthermore, as the shape of the deformation varies from a gaussian shape to a tetter-like shape depending on the excitation parameters, studying the spatiotemporal behaviour of the shape of the deformation induced by ARP should be subject of investigation to carefully characterize the interface deformation through ARP excitation. As the confocal displacement sensor allows tracking the evolution of one point at the water surface over time, this experimental setup could be useful for further work aiming to track the 4D space-time evolution of the surface deformation over time.

AKNOWLEGMENTS

The authors thank J.-P. Rusiecki for his help in the development of the experimental bench. This study has been funded by a regional grant from the University of Tours.

REFERENCES

1. Rayleigh, Lord. XXXIV. *On the pressure of vibrations*. *Lond. Edinb. Dublin Philos. Mag. J. Sci.* **3**, 338–346 (1902).
2. Rooney, J. A. *Nonlinear Phenomena. In: Methods of Experimental Physics*. vol. 19 (New York: Academic, 1981).
3. Lee, C. P. & Wang, T. G. Acoustic radiation force on a bubble. *J. Acoust. Soc. Am.* **93**, 1637–1640 (1993).
4. Löfstedt, R. & Putterman, S. Theory of long wavelength acoustic radiation pressure. *J. Acoust. Soc. Am.* **90**, 2027–2033 (1991).

5. Biquard, P. Les ondes ultra-sonores. *Rev Acoust* **1**, 93 (1932).
6. Hertz, V. G. & Mende, H. Der Schallstrahlungsdruck in Fliissigkeiten. *Zeitschr Phys* **114**, 354–367 (1939).
7. Beyer, R. T. Radiation pressure—the history of a mislabeled tensor. *J. Acoust. Soc. Am.* **63**, 1025–1030 (1978).
8. Chu, B.-T. & Apfel, R. E. Acoustic radiation pressure produced by a beam of sound. *J Acoust Soc Am* **72**, 16 (1982).
9. Rudenko, O. V., Sarvazyan, A. P. & Emelianov, S. Y. Acoustic radiation force and streaming induced by focused nonlinear ultrasound in a dissipative medium. *J. Acoust. Soc. Am.* **99**, 2791–2798 (1996).
10. Kamakura, T., Matsuda, K., Kumamoto, Y. & Breazeale, M. A. Acoustic streaming induced in focused Gaussian beams. *J. Acoust. Soc. Am.* **97**, 2740–2746 (1995).
11. Marston, P. L. Shape oscillation and static deformation of drops and bubbles driven by modulated radiation stresses-Theory. *J Acoust Soc Am* **67**, 15–26 (1980).
12. Marston, P. L., LoPorto-Arione, S. E. & Pullen, G. L. Quadrupole projection of the radiation pressure on a compressible sphere. *J Acoust Soc Am* **69**, 1499–1501 (1981).
13. Yarin, A. L., Pfaffenlehner, M. & Tropea, C. On the acoustic levitation of droplets. *J. Fluid Mech.* **356**, 65–91 (1998).
14. Marston, P. L. & Apfel, R. E. Quadrupole resonance of drops driven by modulated acoustic radiation pressure-Experimental properties. *J Acoust Soc Am* **67**, 27–37 (1980).
15. Asaki, T. J. & Marston, P. L. Equilibrium shape of an acoustically levitated bubble driven above resonance. *J Acoust Soc Am* **97**, 2138–2143 (1995).
16. Callé, S., Remenieras, J.-P., Matar, O. B., Hachemi, M. E. & Patat, F. Temporal analysis of tissue displacement induced by a transient ultrasound radiation force. *J Acoust Soc Am* **118**, 12 (2005).
17. Issenmann, B., Nicolas, A., Wunenburger, R., Manneville, S. & Delville, J.-P. Deformation of acoustically transparent fluid interfaces by the acoustic radiation pressure. *EPL Europhys. Lett.* **83**, 34002 (2008).
18. Calle, S., Ferin, G. & Remenieras, J.-P. Estimation of the radiation force on implanted medical devices: a theorerical study. *Acoust. 2012 Hong Kong* (2012).
19. Lang, R. J. Ultrasonic Atomization of Liquids. *J Acoust Soc Am* **34**, 4 (1962).
20. Baresch, D., Thomas, J.-L. & Marchiano, R. Observation of a single-beam gradient force acoustical trap for elastic particles: acoustical tweezers. *Phys. Rev. Lett.* **116**, 024301 (2016).
21. Devaux, T., Cebrecos, A., Richoux, O., Pagneux, V. & Tournat, V. Acoustic radiation pressure for nonreciprocal transmission and switch effects. *Nat. Commun.* **10**, 3292 (2019).
22. King, L. V. On the acoustic radiation pressure on spheres. *Proc. R. Soc. Lond. Ser. - Math. Phys. Sci.* **147**, 212–240 (1934).
23. Nightingale, K., Soo, M. S., Nightingale, R. & Trahey, G. Acoustic radiation force impulse imaging: in vivo demonstration of clinical feasibility. *Ultrasound Med. Biol.* **28**, 227–235 (2002).
24. Cinbis, C., Mansour, N. N. & Khuri-Yakub, B. T. Effect of surface tension on the acoustic radiation pressure-induced motion of the water–air interface. *J. Acoust. Soc. Am.* **94**, 2365–2372 (1993).
25. Sakai, K., Mizuno, D. & Takagi, K. Measurement of liquid surface properties by laser-induced surface deformation spectroscopy. *Phys Rev E* **63**, 046302 (2001).

26. Trinh, E. H., Marston, P. L. & Robey, J. L. Acoustic Measurement of the Surface Tension of Levitated Drops. *J. Colloid Interface Sci.* **124**, 95–103 (1988).
27. Asaki, T. J., Thiessen, D. B. & Marston, P. L. Effect of an Insoluble Surfactant on Capillary Oscillations of Bubbles in Water: Observation of a Maximum in the Damping. *Phys Rev Lett* **75**, 2686–2689 (1995).
28. Borgnis, F. E. Acoustic Radiation Pressure of Plane Compressional Waves. *Rev. Mod. Phys.* **25**, 653–664 (1953).
29. Kino, G. S. *Acoustic Waves, Devices, Imaging and Analog Signal Processing*. (Prentic-Hall, 1987).
30. F. Coulouvrat. Continuous field radiated by a geometrically focused transducer: Numerical investigation and comparison with an approximate model. *J Acoust Soc Am* **94**, 1663–1675 (1993).
31. Piessens, R. *'Hankel transform' in Transforms and applications handbook*. (A. D. Poularikas CRC, Boca Raton, FL, 2010).
32. Astrath, N. G. C., Malacarne, L. C., Baesso, M. L., Lukasievicz, G. V. B. & Bialkowski, S. E. Unravelling the effects of radiation forces in water. *Nat. Commun.* **5**, 4363 (2014).
33. Xu, Z., Yasuda, K. & Liu, X. Simulation of the formation and characteristics of ultrasonic fountain. *Ultrason. Sonochem.* **32**, 241–246 (2016).
34. Nomura, H. & Shimomura, M. Water surface displacement induced by acoustic radiation pressure of focused ultrasound acting on air-water interface. in Proc. Mtgs. Acoust. 38, 045025 (2019).
35. Komissarova, I. I., Ostrovskaya, G. V. & Shedova, E. N. Light pressure-induced deformations of a free liquid surface. *Opt. Commun.* **66**, 15–20 (1988).
36. Maini, R. Study and Comparison of Various Image Edge Detection Techniques. *Int. J. Image Process.* 13 (2009).
37. Weng, C.-J. *et al.* Confocal displacement sensor with varifocal lens. in *2015 IEEE International Instrumentation and Measurement Technology Conference (I2MTC) Proceedings* 728–733 (IEEE, 2015).
38. Asaki, T. J., Marston, P. L. & Trinh, E. H. Shape oscillations of bubbles in water driven by modulated ultrasonic radiation pressure: Observations and detection with scattered laser light. *J Acoust Soc Am* **93**, 706–713 (1993).
39. Lonzaga, J. B., Osterhoudt, C. F., Thiessen, D. B. & Marston, P. L. Liquid jet response to internal modulated ultrasonic radiation pressure and stimulated drop production. *J Acoust Soc Am* **121**, 3323–3330 (2007).
40. Morse, S. F., Thiessen, D. B. & Marston, P. L. Capillary bridge modes driven with modulated ultrasonic radiation pressure. *Phys. Fluids* **8**, 3–5 (1996).
41. Kornfeld, M. & Triers, V. L. Swelling of a liquid surface under the influence of ultrasound. *Sov Phys Tech Phys* **26**, 2778 (1956).

Journal of Applied Physics

AIP Publishing

Journal of Applied Physics

AIP Publishing

AIP Publishing

Journal of Applied Physics

ACCEPTED MANUSCRIPT

PLEASE CITE THIS ARTICLE AS DOI: 10.1063/5.0112969

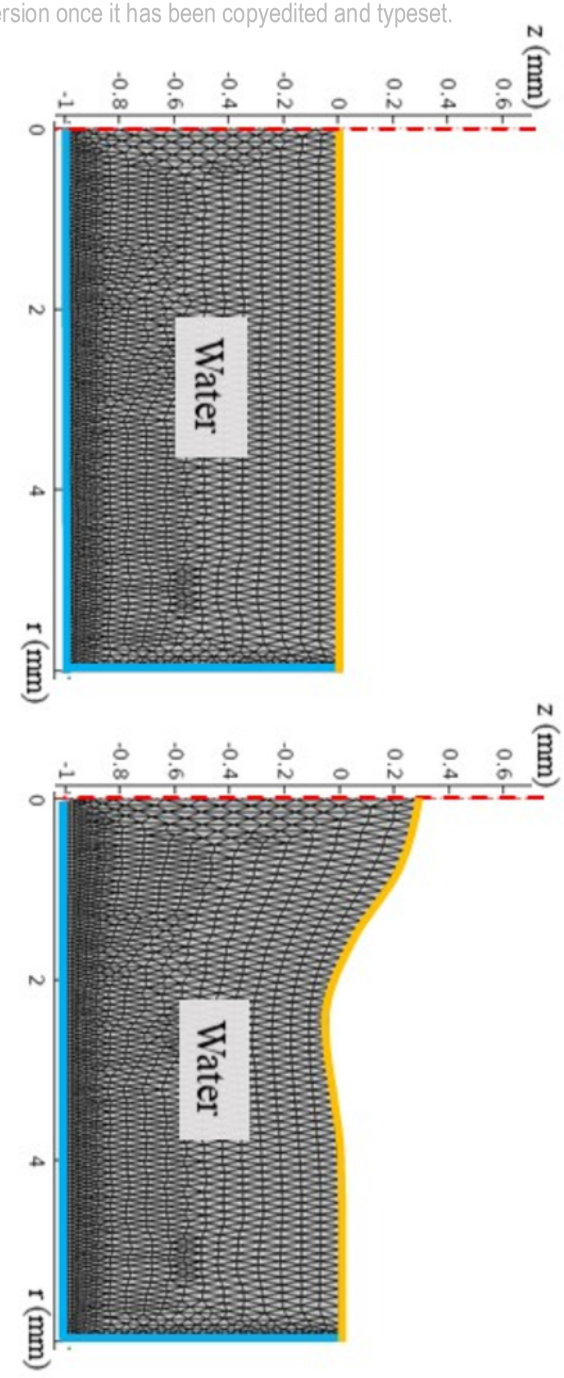

AIP Publishing

Journal of Applied Physics

PLEASE CITE THIS ARTICLE AS DOI: 10.1063/5.0112969

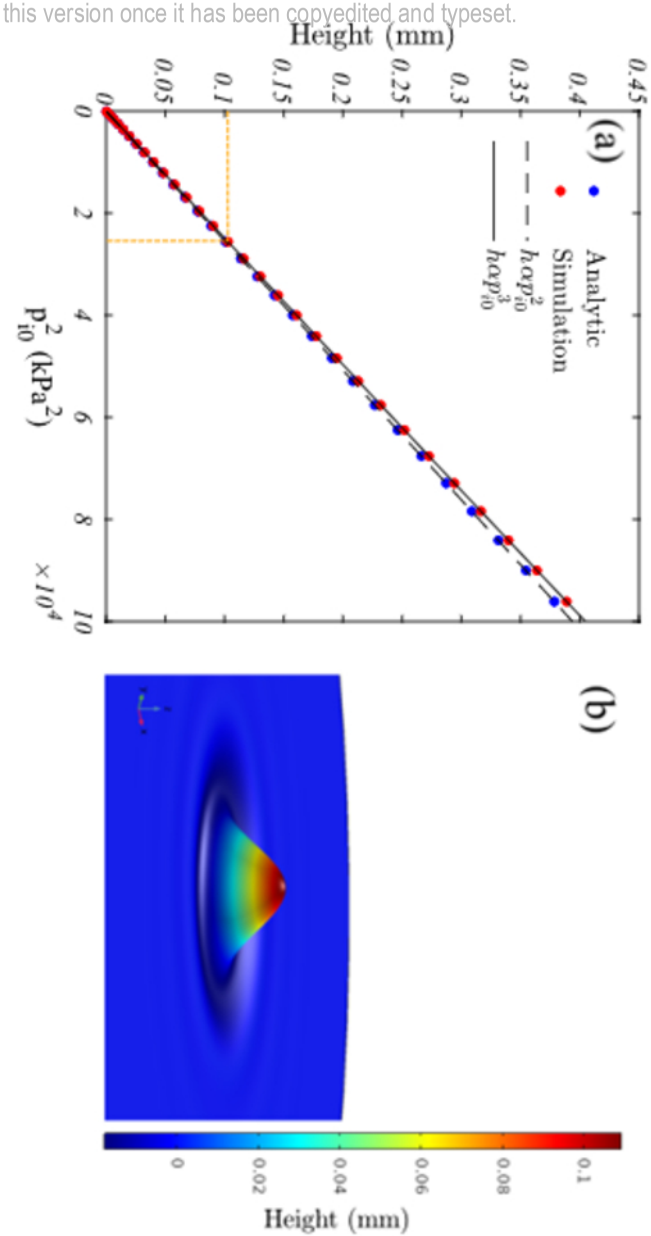

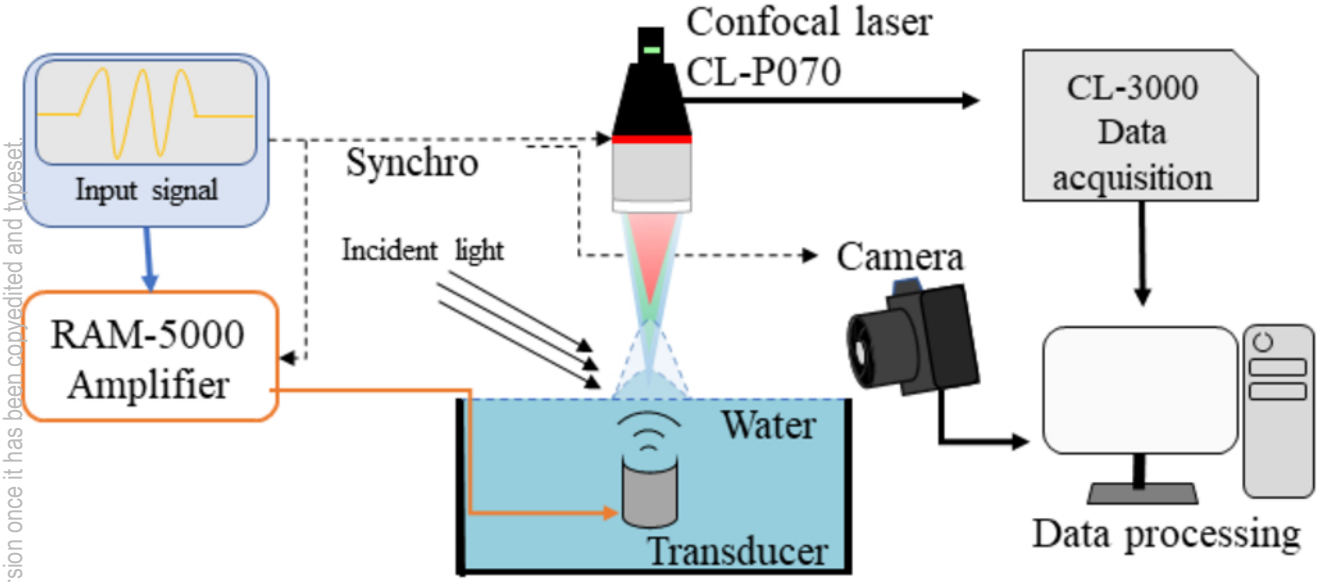

Journal of Applied Physics
AIP Publishing

Journal of Applied Physics

AIP Publishing

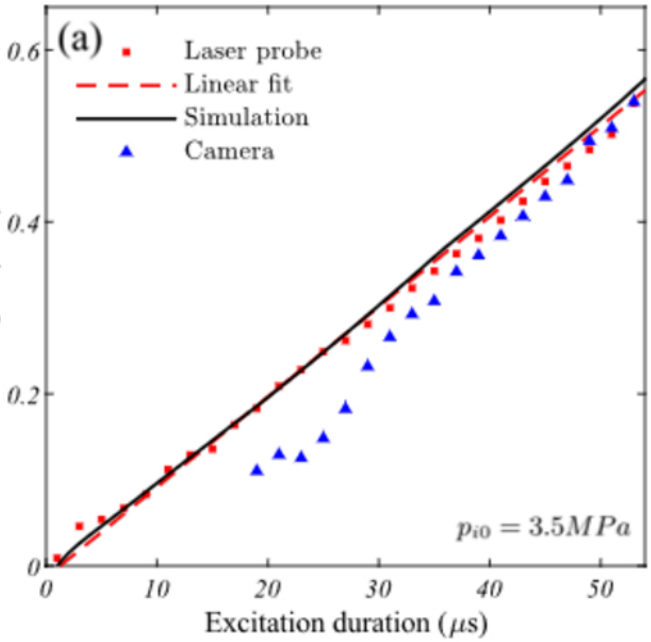

Journal of Applied Physics
AIP Publishing

Journal of Applied Physics

AIP Publishing

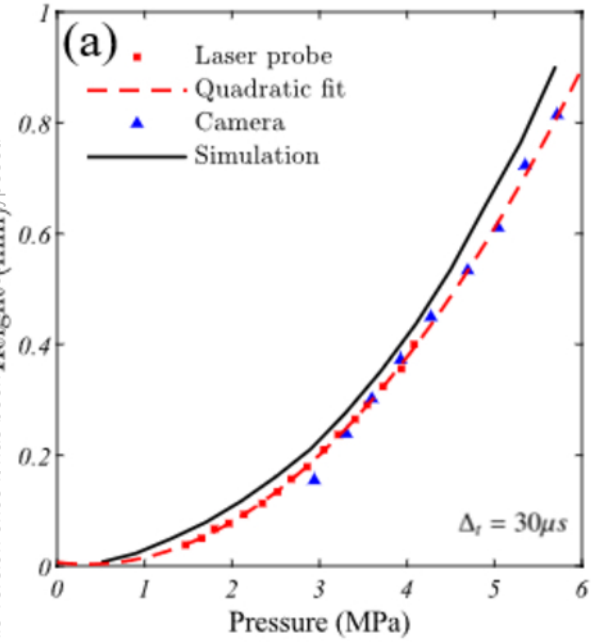

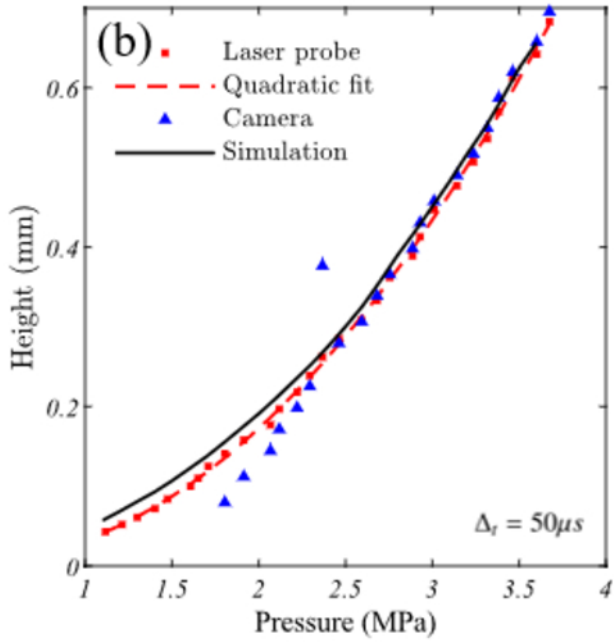

Journal of Applied Physics

AIP Publishing

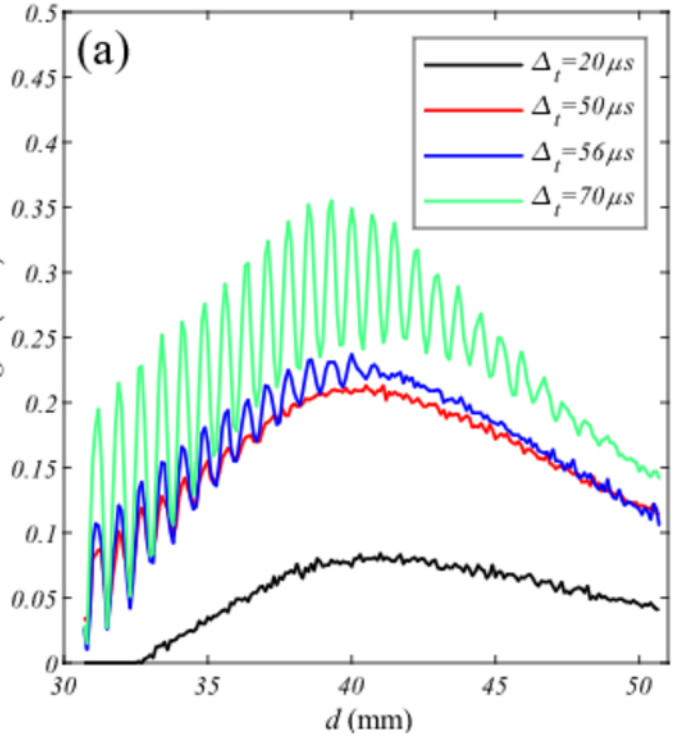

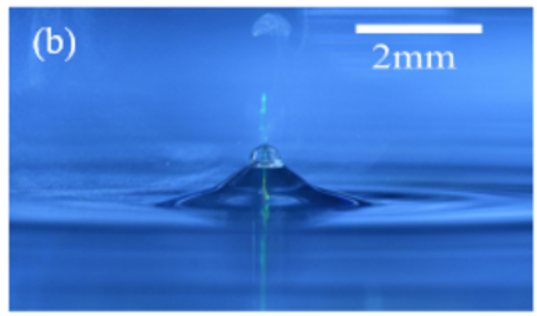

Journal of Applied Physics

AIP Publishing